Nonlinearity-driven topology via spontaneous symmetry breaking

Alessandro Coppo [1,2,*] Alexandre Le Boité [3] Simone Felicetti [1,2] and Valentina Brosco [1,2]
[1] *Istituto dei Sistemi Complessi, Consiglio Nazionale delle Ricerche, Via dei Taurini, 19 I-00185 Rome, Italy*
[2] *Physics Department, University of Rome, "La Sapienza", P.le A. Moro, 2 I-00185 Rome, Italy*
[3] *Université Paris Cité, CNRS, Matériaux et Phénomènes Quantiques, F-75013 Paris, France*

(Received 31 March 2025; revised 22 October 2025; accepted 4 March 2026; published 8 April 2026)

Topology and nonlinearity are deeply connected. However, whether topological effects can arise solely from the structure of nonlinear interaction terms, and the nature of the resulting topological phases, remain to large extent open questions. Here we consider a chain of parametrically driven quantum resonators coupled only via weak nearest-neighbor cross-Kerr interaction, without any quadratic tunneling term. We show that, when the drive overcomes a critical threshold value, the system undergoes a transition from the atomic limit of decoupled oscillators to a symmetry-broken topological phase. The topology is determined by the interplay of local and nearest-neighbor Kerr nonlinearities, yielding a nontrivial bulk-boundary correspondence. In the topological phase, we derive analytical approximations for the low-energy spectrum, identifying the conditions to observe topological edge modes.

DOI: 10.1103/q2br-g63y

In classical and quantum many-body systems, phase transitions between states with different symmetries are described by local order parameters. The scaling properties of these parameters near the transition allow for the identification of universal features and the classification of critical behavior [1]. Unlike symmetry-breaking phases, topological phases are defined not by local order parameters but by global topological invariants [2–4]. In the absence of nonlinearities, topological band theory provides a unifying framework for characterizing topological phases in quantum materials [5] and photonic systems [6] enabling the description of topological phenomena such as quantized transport [7,8] and gapless edge states [9,10].

Going beyond quadratic Hamiltonians, nonlinear interactions can profoundly influence topological systems [11]. For example, interactions can modify or destroy existing topological effects [12–14], perturb boundary modes [15–17], or give rise to topologically ordered phases [18–23]. These phenomena demonstrate the deep connection between topology and nonlinearity. However, whether topological effects can arise solely from the structure of nonlinear interaction terms, and the nature of the resulting topological phases, remain to large extent open questions. Aside from its fundamental relevance, answering these questions is crucial to properly characterize topological effects and discover novel topological materials.

Quantum resonators are ideal systems for exploring both topological properties [24] and nonlinear quantum phenomena [25,26]. In these systems, driven-dissipative quantum phase transitions are striking manifestations of nonlinearity as experimentally demonstrated in Refs. [27–31] following the prediction of Refs. [32–36]. Specifically, when the quadratic part of the effective resonator potential becomes unstable, quantum resonators display a finite-component quantum phase transition [37–39]. Nonlinearities, even vanishingly small, are then essential in establishing a stable phase [40]. Upon crossing the critical point, the system transitions from a low-excitation phase, to a symmetry-broken highly populated state.

Parametric quantum resonators are a class of systems where such instabilities occur and typically originate from two-photon generation processes. They can be realized in a variety of settings [35] ranging from nanomechanical systems [35,41] to optical oscillators [42–45] and superconducting circuits [31]. Their applications range from the encoding of Schrödinger cat qubits [46–48], to quantum sensing [49–52] and large-scale simulations [53]. In all these frameworks, systems of multiple parametric quantum resonators have been shown to enable novel interesting functions including dissipative bath engineering [54], hyperspin encoding [55], and collective quantum sensing [56] as well as the simulation of nonequilibrium quantum phases [57]. Several models have been proposed in recent years to investigate topological properties in arrays of bosonic resonators. These models extend standard topological tight-binding Hamiltonians by adding parametric processes [58,59], counter-rotating terms [60], local nonlinear interactions [61–64], and the breaking of time-reversal symmetry through external fields [65,66].

In this work, we adopt an alternative approach and investigate a setting in which effective topological bands emerge from spontaneous symmetry breaking (SSB) across a finite component quantum phase transition in each resonator of the lattice. We consider a chain of parametric quantum resonators

*Contact author: alessandro.coppo@cnr.it

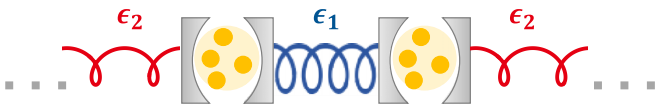

FIG. 1. Model. Sketch of the parametric quantum resonator chain with staggered cross-Kerr interactions [see Eqs. (1) and (2)].

featuring weak nonlinearities, local Kerr and staggered cross-Kerr terms, without any direct quadratic coupling between the resonators. We focus on the properties of the system above threshold, where the quadratic potential is unstable. We show that nonlinear interaction terms can induce a transition from the *atomic limit* of decoupled oscillators to a nontrivial *topological phase*. We analyze the nature of the emerging Bogoliubov bosonic oscillations around equilibrium solutions. The system features different equilibrium phases including a density-wave phase characterized by localized excitations, and a homogeneous phase with dispersive Bogoliubov modes described by a Hamiltonian whose bulk structure is reminiscent of the Su-Schrieffer-Heeger (SSH) model [67]. Interestingly, this Hamiltonian displays parametric tunneling terms and is not homogeneous along the chain, yielding nontrivial topological properties and bulk-boundary correspondence.

This paper is organized as follows. In Sec. I, we define the Hamiltonian for the chain of nonlinear resonators illustrated in Fig. 1 and discuss the relevant parameter space. In Sec. II, we analyze the single-cell phase diagram to characterize the phase transition, the fundamental mechanism underlying the emergent topological properties of the lattice. In Sec. III, we derive analytical solutions for the bulk ground states and demonstrate the onset of a nontrivial Zak phase within the symmetry-broken regime. The properties of the localized edge modes are examined in Sec. IV. Finally, concluding remarks and the broader implications of this work are presented in Sec. V.

I. MODEL

We consider a chain of $2N$ Kerr resonators with frequency ω and parametric driving λ, as sketched in Fig. 1. We assume that nearest-neighbor resonators are coupled only *via* cross-Kerr interaction terms. Introducing bosonic creation and annihilation operators, the system Hamiltonian can thus be written as the sum of two terms as $H = H_L + H_C$ where H_L describes a chain of decoupled parametric Kerr resonators ($\hbar = 1$)

$$H_L = \sum_{\substack{1\leqslant n\leqslant N \\ I\in\{A,B\}}} \left[\omega\, c_{In}^\dagger c_{In} + \frac{\lambda}{2}(c_{In}^\dagger c_{In}^\dagger + \text{H.c.}) + \epsilon_L\, c_{In}^\dagger c_{In}^\dagger c_{In} c_{In}\right], \tag{1}$$

while H_C accounts for cross-Kerr nonlinearities,

$$H_C = \sum_{n=1}^{N} [\epsilon_1\, c_{An}^\dagger c_{An} c_{Bn}^\dagger c_{Bn} + \epsilon_2\, c_{An+1}^\dagger c_{An+1} c_{Bn}^\dagger c_{Bn}], \tag{2}$$

where we note that the local Kerr intensity ϵ_L is homogeneous while the cross-Kerr nonlinearity has a staggered structure. Starting from the Hamiltonian H we can define three adimensional parameters, respectively indicated as g, μ, and δ, that govern the physics of the model. The parameter g sets the distance from the instability for each resonator and it reads as

$$g^2 = \frac{\lambda - \omega}{2\epsilon_L} \tag{3}$$

with $\lambda > \omega$. The parameters μ and δ define the structure of the nonlinearity and they are given by

$$\mu = \frac{\epsilon_2 + \epsilon_1}{2\epsilon_L} \quad \text{and} \quad \delta = \frac{\epsilon_2 - \epsilon_1}{\epsilon_2 + \epsilon_1}. \tag{4}$$

II. SINGLE CELL

To understand how the topological symmetry-broken phase emerges, it is useful to start by setting the intercell cross Kerr to zero $\epsilon_2 = 0$ and considering a single resonator pair. The ground state $|G\rangle$ can be obtained by exact numerical simulations. We plot in Fig. 2 the squared modulus of the Husimi function $Q(\alpha, \beta) = \langle\alpha, \beta|G\rangle$ for different values of the ratios λ/ω and μ, with $\alpha, \beta \in \mathbb{C}$ identifying the coherent states of the two resonators.

For $\lambda \ll \omega$ the ground state is essentially the vacuum and $Q(\alpha, \beta)$ is a Gaussian centered in $\alpha = \beta = 0$ as shown in Fig. 2(a). As λ increases, the ground state becomes more and more squeezed. However, as long as $\lambda < \omega$, the function $Q(\alpha, \beta)$ remains localized around $\alpha = \beta = 0$. When λ overcomes the threshold ω, the vacuum state becomes unstable and three distinct regimes emerge, as illustrated in Figs. 2(b)–2(d).

When cross-Kerr interaction dominates over the local one, i.e., for $\mu > 1$, $Q(\alpha, \beta)$ has of four maxima located at $\{\pm ig, 0\}$ and $\{0, \pm ig\}$, as shown in Fig. 2(d). In this case, it is energetically favorable to frustrate cross-Kerr interaction by creating an inhomogeneous semiclassical ground state, consistent with the findings of Ref. [68]. In this regime, each lobe of the Husimi function represents a single-mode squeezed state, and the corresponding quadratic Hamiltonian does not couple modes in the two resonators.

When the local Kerr interaction dominates, for $\mu < 1$, both resonators are equally excited and the maxima of $Q(\alpha, \beta)$ shift to $\{\pm i\bar{g}, \pm i\bar{g}\}$, where $\bar{g}^2 = g^2/(\mu + 1)$, as depicted in Fig. 2(b). In this regime, each lobe of the Husimi function represents a two-mode squeezed state, indicating an effective coupling between the two resonators in the quadratic Hamiltonian. Eventually, for $\mu = 1$, the maxima of the Husimi function lie on a circle of radius $\bar{g}$ as shown in Fig. 2(c). Figure 2 therefore illustrates how, for $\epsilon_2 = 0$, the structure of the ground state, the squeezing properties, and consequently the nature of the Bogoliubov excitations change across the three regimes.

III. FULL CHAIN

A similar symmetry-breaking transition is observed in the extended system, when the intercell cross-Kerr terms are present $\epsilon_2 \neq 0$. In this case, the homogeneous and inhomogeneous regimes are reminiscent of the homogeneous and density wave phases found in the extended Bose-Hubbard model in the limit of vanishingly small tunneling [69,70].

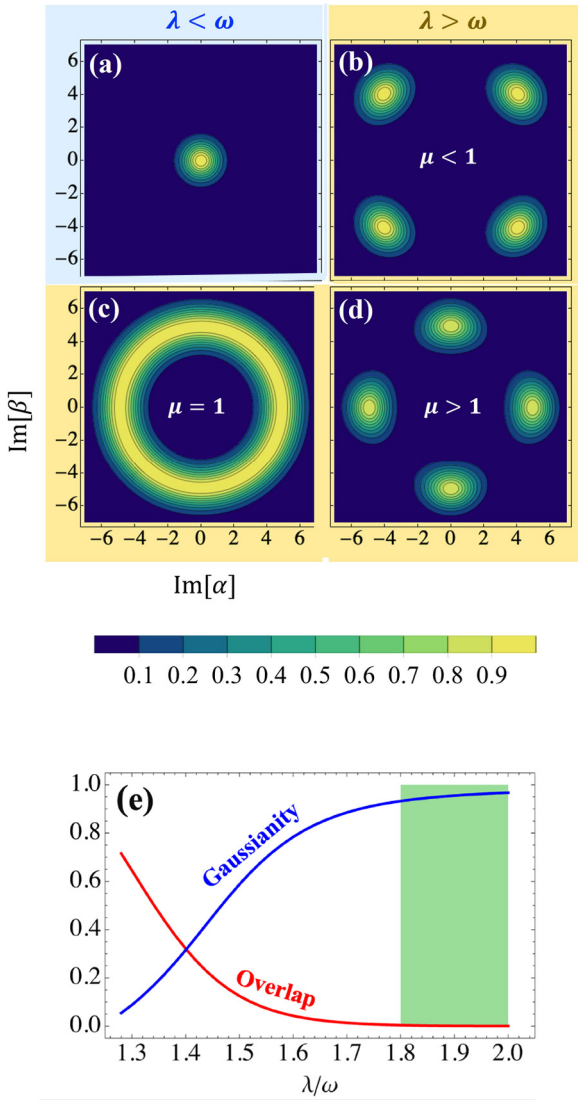

FIG. 2. Single-cell Husimi function. (a)–(d) Ground state Husimi function of a pair of resonators. Parameter values: (a) $\lambda = 0$ and $\epsilon_1 = \epsilon_L$; (b)–(d) $\lambda = 2\omega$ and, $\epsilon_1 = \epsilon_L$ (b), $\epsilon_1 = 2\epsilon_L$ (c), and $\epsilon_1 = 3\epsilon_L$ (d). In all panels we set $\epsilon_L = 0.02\ \omega$. Numerical results obtained with 50 Fock states per resonator, Husimi function normalized to its maximum. (e) Normalized interlobe weight (red) and KL divergence with a Gaussian ensemble (blue). The SSB regime is highlighted in green.

To investigate the emergence of the topological phase, we focus on the homogeneous regime $\mu < 1$ that features an effective quadratic coupling between the resonators above threshold, as it will be clear in the following. To derive analytical solutions, we will take the limit in which all Kerr and cross-Kerr nonlinearities are small, and the low-energy spectrum is well described by a Gaussian approximation [40]. Fluctuations beyond this approximation arise from two main sources: the overlap between different lobes of the Husimi function and non-Gaussian features within each lobe. The validity of the Gaussian approach can therefore be assessed by estimating two quantities defined for a pair neighboring resonators. The first is the normalized interlobe weight $\max_\beta |Q(0,\beta)|^2 / \max_{(\alpha,\beta)} |Q(\alpha,\beta)|^2$, describing the overlap between adjacent lobes, and the second is the Kullback-Leibler divergence between the Husimi function and the corresponding Gaussian ensemble, serving as Gaussianity test. The results, shown in Fig. 2(e) for different values of the ratio λ/ω, demonstrate that the Gaussian description is accurate sufficiently far from the instability.

Within the Gaussian framework, we start by determining the semiclassical equilibrium points which identify the positions of the maxima of the Husimi function. We thus introduce the displaced operators

$$c_{An} = d_{An} - \alpha_n \quad \text{and} \quad c_{Bn} = d_{Bn} - \beta_n \tag{5}$$

in the Hamiltonian H and we choose the complex numbers α_n and β_n so that all terms linear in d_{An} and d_{Bn} vanish and the resulting quadratic Hamiltonian is positive definite. By doing so one can show that α_n and β_n are purely imaginary and satisfy the following equations:

$$2|\alpha_n|^2 + \mu(1-\delta)|\beta_n|^2 + \mu(1+\delta)|\beta_{n-1}|^2 = 2g^2, \tag{6}$$

$$2|\beta_n|^2 + \mu(1-\delta)|\alpha_n|^2 + \mu(1+\delta)|\alpha_{n+1}|^2 = 2g^2. \tag{7}$$

The above equations are invariant under $\alpha_n \to -\alpha_n$ and $\beta_n \to -\beta_n$ yielding 2^{2N} degenerate semiclassical ground states. This degeneracy stems from the boson-parity preserving nature of the Hamiltonian H.

When the system is sufficiently far from the transition, $\bar{g} \gg 1$, the Husimi function of the chain consists of 2^{2N} disconnected lobes, analogous to the two-resonator case shown in Fig. 2(b). In this regime, we can describe the dynamics of Gaussian fluctuations around single semiclassical solutions by a quadratic Hamiltonian of the form

$$\begin{aligned} H_2 = \sum_n \Bigg\{ \sum_I \left[\Omega_{In} d_{In}^\dagger d_{In} + \frac{\Lambda_{In}}{2}(d_{In}d_{In} + \text{H.c.}) \right] \\ + [J_{1n}(d_{An}^\dagger d_{Bn} - d_{An}d_{Bn}) + J_{2n}(d_{An+1}^\dagger d_{Bn} - d_{An+1}d_{Bn}) \\ + \text{H.c.}] \Bigg\}, \end{aligned} \tag{8}$$

where the tunneling terms J_{1n} and J_{2n} are given by $J_{1n} = \epsilon_1|\alpha_n\beta_n|$ and $J_{2n} = \epsilon_2|\alpha_{n+1}\beta_n|$, while the renormalized frequencies and driving amplitudes read as $\Omega_{An} = \lambda + 2\epsilon_L|\alpha_n|^2$ and $\Lambda_{An} = \lambda - 2\epsilon_L|\alpha_n|^2$. Analogous relations hold for Ω_{Bn} and Λ_{Bn} with α_n replaced by β_n. The particular choice of the symmetry-broken semiclassical ground state, e.g., satisfying $\text{Im}[\alpha_n] = \text{Im}[\beta_n] > 0$, only affects the phase of the tunneling term and the squeezing direction and it can be reabsorbed in a redefinition of the d_{In} operators. What is more important, the amplitudes α_n and β_n, solving Eqs. (6) and (7), are larger near the edge sites and decay to a constant in the bulk, as shown in Fig. 3(a).

This implies that the Hamiltonian H_2 has an inhomogeneous structure along the chain which alters its symmetries. In particular, even at small μ, H_2 does not preserve the chiral symmetry but retains the inversion symmetry defined by $a_n \to b_{N+1-n}$, $b_n \to a_{N+1-n}$. These unconventional symmetry properties play a crucial role in the topological classification of the system and allow to interpret the boundary behavior of H_2 within the framework of fragile topological

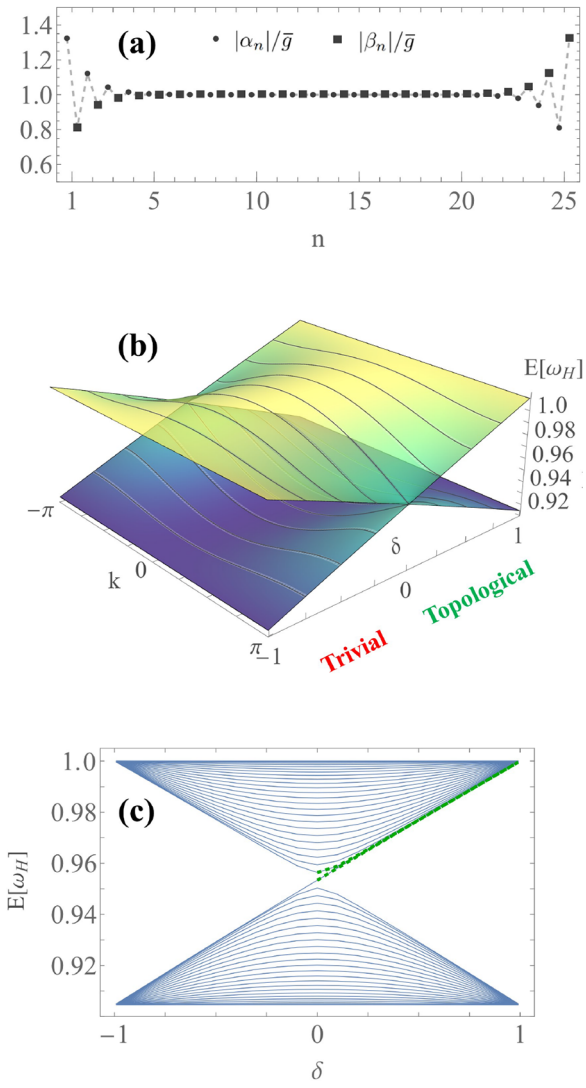

FIG. 3. Full-chain semiclassical ground state and spectrum. (a) The semiclassical solutions $|\alpha_n|$ and $|\beta_n|$ for $\mu = 0.9$, $\delta = 0.5$, and $N = 25$ cells. (b) Bulk band structure as a function of δ for $\mu = 0.1$. (c) Spectrum as a function of δ for $\mu = 0.1$ and $N = 25$. Each line identifies an energy level. Dashed green lines indicate quasidegenerate levels emerging near the upper band.

insulators [15,71,72]. In this setting, topology manifests via a spectral flow across the energy gap, as illustrated by the dashed green lines in Fig. 3(c), when δ is tuned from negative to positive values. Boundary modes in the middle of the gap are instead absent. The amplitude of the gap and the overall structure of spectrum of the Hamiltonian H_2 depend on both the parameter μ and δ which, controlling the structure of the interaction terms, determine the correlation length of the semiclassical solution as shown in the Appendix A. In particular, for small μ, one can define a wide bulk region where H_2 is homogeneous and can be diagonalized by switching to k space and performing a Bogoliubov transformation. By doing so, in Appendix A, up to constant terms, in the bulk we obtain $H_2 = \sum_{k,\eta} \mathcal{E}_k^\eta C_{\eta k}^\dagger C_{\eta k}$ where $C_{\eta k}^\dagger$ and $C_{\eta k}$ with $\eta \in \{+,-\}$ are creation and annihilation operators of Bogoliubov excitations, and the energies $\mathcal{E}_k^\pm$ can be cast as

$$\mathcal{E}_k^\pm = \omega_H \sqrt{\frac{1}{1+\mu}\left(1 \pm \mu \sqrt{\frac{1+\delta^2}{2} + \frac{1-\delta^2}{2}\cos k}\right)}, \quad (9)$$

with $\omega_H = 2\sqrt{\lambda(\lambda - \omega)}$. The spectrum of Bogoliubov excitations has a gap $\Delta \simeq \mu|\delta|$ that vanishes for $\epsilon_2 = \epsilon_1$, as shown in Fig. 3(b). The topological properties of the two bands for $\delta \neq 0$ can be then characterized via the Zak phase

$$\phi_{\text{Zak}}^\eta = i \int_{-\pi}^{\pi} \frac{dk}{\pi} \langle G | C_{\eta k}\, \partial_k C_{\eta k}^\dagger | G \rangle, \quad (10)$$

where $|G\rangle$ denotes the ground state of H_2. In Appendix A we obtain $\phi_{\text{Zak}}^\pm = \pm 1$ for $\delta > 0$ and $\phi_{\text{Zak}}^\pm = 0$ for $\delta < 0$, reminiscent of the SSH model. However, differently from the SSH model, a nonvanishing ϕ_{Zak} does not correspond to the emergence of protected modes at the boundaries due to the absence of chiral symmetry. Instead, as discussed above, the system exhibits a spectral flow [72]. This manifests in the appearance of two additional levels aligned with the lower edge of the upper band for $\epsilon_2 \gg \epsilon_1$. These levels are degenerate due to inversion symmetry but are not protected by the gap, and their wave functions extend over the entire lattice.

The emergence of these levels can be understood focusing on the limit $\delta = 1$. In this case, the Hamiltonian H describes a chain composed of $N - 1$ resonator pairs, forming the bulk, and two isolated sites at the edges. In the bulk pairs, SSB leads to the appearance of a bosonic "Higgs-like" mode, whose energy ω_H does not depend on the strength of the nonlinear interactions, according to Eq. (9), and of a "Goldstone-like" mode with energy $\omega_H\sqrt{(1-\mu)/(1+\mu)}$, vanishing in the limit $\mu = 1$. The edge sites instead have a single mode with energy ω_H. Consequently, at $\delta = 1$, the edge mode and the Higgs-like bulk modes are degenerate. In this scenario any finite value of ϵ_1 couples all degenerate modes causing the spreading of the edge modes across the whole chain (see Appendix B).

We refer to the bulk modes as "Higgs" and "Goldstone" since, for $\mu = 1$, they arise from the breaking of the continuous O(2) symmetry, as displayed in Fig. 2(d), and reminiscent of the SSB in the sigma model yielding a massive "Higgs" boson, with mass independent of the quartic term (at tree level), and a massless Goldstone boson [73,74].

As we noted above, at $\mu = 1$ the ground state of the system changes from a density wave to a homogeneous phase. Interestingly, this point also marks a transition in the nature of the Gaussian modes which are nondispersive and nontopological in the density-wave phase. We note in particular that for $\mu > 1$, a homogeneous ground state would lead to an unstable lower band as one can understand by looking at Eq. (9), analogous to what happens in the dimer. The topology of the Gaussian Hamiltonian (8) is thus not a trivial consequence of the staggered structure of the nonlinear interaction terms but arises from a delicate interplay of correlation and spontaneous symmetry breaking. The peculiar mechanism leading to the inhomogeneous structure of the Gaussian Hamiltonian, stemming from the nonlocal nature of the nonlinearities and responsible for the emergence of fragile topology, may extend beyond the weakly interacting regime. For instance, boundary effects become particularly pronounced in strongly correlated

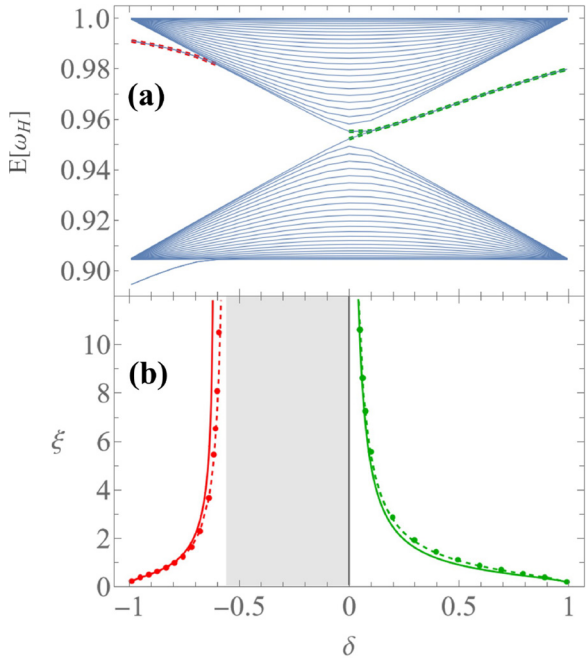

FIG. 4. Restoring the bulk-boundary correspondence. (a) Spectrum as a function of δ for $\mu = 0.1$, $N = 25$, and $\delta_\lambda = 0.02\,\lambda$. The dashed green and red lines indicate topological and impurity-induced boundary modes, respectively. (b) Dependence on δ of the correlation length ξ in the two cases. Solid lines are analytical fits given, for topological modes, by the SSH-like behavior, and, for impurity induced, by perturbation theory.

systems, where screening is typically more efficient in the bulk (see, e.g., [75,76]) and correlations are naturally nonlocal, supporting the view that the phenomenology discussed here could, under suitable conditions, persist in strongly interacting regimes.

IV. EDGE MODES

The fragile nature of the topological phase of system ultimately stems from the degeneracy of the edge and Higgs-like bulk modes, which, in turn, arises from the nonhomogeneous structure of H_2, it should be possible to restore it by introducing a small nonuniform correction to the quadratic part of the Hamiltonian H, thereby making H_2 more homogeneous. This can be achieved by reducing the driving on the left and right boundary sites by adding the following term to H:

$$\delta H_\lambda = -\delta_\lambda \left(c_{A1}^\dagger c_{A1}^\dagger + c_{BN}^\dagger c_{BN}^\dagger + \text{H.c.}\right), \tag{11}$$

with $\delta_\lambda \ll \lambda$. The correction δH_λ modifies the structure of the semiclassical ground state, leading to the emergence of two isolated modes in the spectrum of the quadratic Hamiltonian, as shown in Appendix B and in Fig. 4(a) for $\delta_\lambda = 0.02\,\lambda$. These modes appear both around $\delta = 1$ and -1. In the topological phase ($\delta > 0$), the two modes remain isolated from the rest of the spectrum. In contrast, in the topologically trivial phase ($\delta < 0$), they stay isolated only as long as $\epsilon_2 \lesssim \delta_\lambda$. This highlights the different effect of the correction δH_λ in the two phases. To understand this point it is useful to consider the behavior of the semiclassical ground state of H close to $\delta = -1$ and 1. In the first case, it is homogeneous and a finite δ_λ introduces an impurity, giving rise to nontopological localized modes. On the other hand, as explained above, at $\delta = 1$ the ground state is inhomogeneous, therefore introducing δH_λ reduces the inhomogeneity and favors the emergence of the topological modes. The different origins of the localization in the two phases describes a nontrivial bulk-boundary correspondence which is captured by the behavior of the localization length ξ, as shown in Fig. 4(b). In the topological phase, ξ follows an SSH-like behavior $\xi^{-1} \propto \log(\epsilon_2/\epsilon_1)$, whereas in the trivial phase, standard perturbation theory yields a correlation length which diverges when δ reaches a threshold value (see Appendix B).

V. CONCLUSION

In this work, we considered a nonlinear many-body bosonic chain where parametric driving induces a quantum phase transition. In the symmetry-broken phase, the presence of staggered cross-Kerr terms gives rise to an emergent fragile topological phase characterized by a spectral flow. These results demonstrate that topological effects may arise not only from standard quadratic tunnelings but also from nonlinear interaction terms. The conceptual relevance of the results thus goes far beyond the simple model studied here, and extends to more complex topological structures characterized by different symmetries, dimensions, and interaction regimes. Among the most interesting extensions, the dissipative case is essential for the realistic modeling of physical systems. Experiments carried in various platforms already demonstrated the SSB transition for dissipative resonators [27–31] and for Rabi systems [77,78]. In these cases, the steady state of the open system and the ground state of the underlying closed system [37–40] have remarkable similarities. Accordingly, we expect that the mechanism for nonlinearity induced topology discussed in this work will not be hindered by dissipation. The mechanism studied here could then give rise to a rich variety of nonlinear driven-dissipative topological phenomena.

ACKNOWLEDGMENTS

We acknowledge useful discussions with B. van Heck and D. Guerci. A.C., S.F., and V.B. acknowledge financial support from PNRR MUR Project No. PE0000023-NQSTI financed by the European Union–Next Generation EU. S.F. acknowledges support from CQSense project financed by Fondazione Compagnia di San Paolo.

DATA AVAILABILITY

No data were created or analyzed in this study.

APPENDIX A: PERIODIC CHAIN

In this appendix, we provide details regarding the results for the chain under periodic boundary conditions (PBC) and show that, for small values of μ, these results also hold for open boundary conditions (OBC) in a wide bulk region where the semiclassical solution remains homogeneous.

1. Semiclassical ground state

Let us consider the chain of $2N$ nearest-neighbor Kerr resonators described by Eqs. (1) and (2). For $\lambda \gg \omega$ and $\mu < 1$, the amplitudes α_n, β_n identifying the semiclassical ground states are purely imaginary and satisfy Eqs. (6) and (7). It is useful to define the parameter $\tau > 0$ via

$$\sinh^2\left(\frac{1}{2\tau}\right) = \frac{1/\mu^2 - 1}{1-\delta^2}, \tag{A1}$$

and rewrite the equations as

$$\frac{1}{4\sinh^2\left(\frac{1}{2\tau}\right)}\left(|\alpha_{n+1}|^2 + |\alpha_{n-1}|^2 - 2|\alpha_n|^2\right) - |\alpha_n|^2 + \bar{g}^2 = 0 \tag{A2}$$

for $n = 2, \ldots, N$, and

$$|\beta_n|^2 = g^2 - \mu\left[\frac{1-\delta}{2}|\alpha_n|^2 + \frac{1+\delta}{2}|\alpha_{n+1}|^2\right] \tag{A3}$$

for $n = 1, \ldots, N$. In general, Eq. (A2) is solved by

$$|\alpha_n|^2 = \bar{g}^2 + c_1\, e^{-n/\tau} + c_2\, e^{n/\tau}, \tag{A4}$$

with the constants c_1, c_2 fixed by OBC, i.e., $\alpha_{N+1} = 0$ and $\beta_0 = 0$. The parameter τ thus takes the meaning of a correlation length which describes the semiclassical ground-state inhomogeneity along the chain. Using Eqs. (6) and (7), the condition $\beta_0 = 0$ can be rewritten as

$$g^2\left(1 - \mu\frac{1-\delta}{2}\right) = \left[1 - \mu^2\left(\frac{1-\delta^2}{2}\right)^2\right]|\alpha_1|^2 - \mu^2\frac{1-\delta^2}{4}|\alpha_2|^2. \tag{A5}$$

Substituting into Eq. (A4) and considering also Eq. (A3), we find

$$|\alpha_n|^2 = \bar{g}^2\left[\frac{4}{R}\sinh\left(\frac{N+1-n}{\tau}\right) + 1 - e^{-\left(\frac{N+1-n}{\tau}\right)}\right],$$
$$|\beta_n|^2 = |\alpha_{N+1-n}|^2, \tag{A6}$$

with $R = \mu\, e^{N/\tau}[(1-\delta)\, e^{1/\tau} + (1+\delta)]$. Figure 5 shows that the correlation length τ can be used to determine the extension of a "bulk region," where the ground state stays essentially homogeneous, i.e., $|\alpha_n|^2 \sim |\beta_n|^2 \sim \bar{g}^2$. Note that the length τ depends on μ and δ as shown in Fig. 6. When μ approaches 1, τ exponentially increases and the size of the bulk region is reduced. On the other hand, if $\mu \ll 1$, τ tends to zero and all the chain, except the first and last sites, can be considered as the bulk.

Note that, as one would expect, the mentioned homogeneous bulk solution can be obtained by neglecting boundary effects and imposing PBC

$$\alpha_{N+1} = \alpha_1,$$
$$\alpha_N = \alpha_0, \tag{A7}$$

which, substituting into Eq. (A4), yields to $c_1 = c_2 = 0$ such that

$$|\alpha_n|^2 = |\beta_n|^2 = \bar{g}^2. \tag{A8}$$

The second line of Eq. (A7) is equivalent to $\beta_N = \beta_0$ via Eq. (A3).

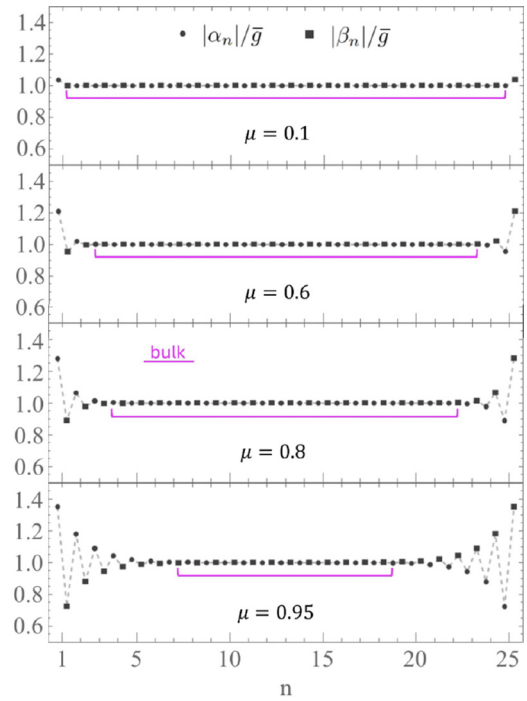

FIG. 5. The OBC semiclassical ground states for a chain of $N = 25$ cells with $\delta = 0.5$ and different values of μ. The magenta lines indicates the bulk regions, $10\,\tau \lesssim n \lesssim N + 1 - 10\,\tau$.

2. Quadratic Hamiltonian

According to Eq. (8), in the case of PBC and for $\mu < 1$, the quadratic Hamiltonian describing Gaussian fluctuations around a single semiclassical ground state can be cast as

$$H_2 = \sum_{n=1}^{N}\Bigg\{\sum_{I\in\{A,B\}}\left[\Omega\, d_{In}^\dagger d_{In} + \frac{\Lambda}{2}(d_{In}d_{In} + \text{H.c.})\right] + [J_1(d_{An}^\dagger d_{Bn} - d_{An}d_{Bn}) + J_2(d_{A,n+1}^\dagger d_{Bn} - d_{A,n+1}d_{Bn}) + \text{H.c.}]\Bigg\} \tag{A9}$$

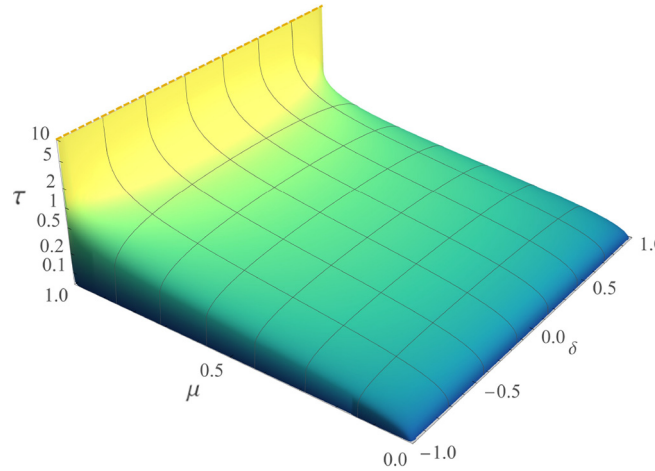

FIG. 6. The correlation length τ as a function of μ and δ (logarithm scale).

with

$$\Omega = \lambda + \frac{\lambda-\omega}{1+\mu}, \quad \Lambda = \lambda - \frac{\lambda-\omega}{1+\mu},$$
$$J_1 = \frac{\mu(\lambda-\omega)}{1+\mu}\frac{1-\delta}{2}, \quad J_2 = \frac{\mu(\lambda-\omega)}{1+\mu}\frac{1+\delta}{2}. \quad \text{(A10)}$$

Given the PBC $d_{AN+1} = d_{A1}$, $d_{BN} = d_{B0}$, and, being all the parameters in (A9) homogeneous, it is natural to switch to the k space via the discrete Fourier transform. We thus define the ladder operators $d_{Ik} = N^{-1/2}\sum_n d_{In}\, e^{-ikn}$, with $k = 2s\pi/N$ restricted to the first Brillouin zone (FBZ), i.e., $s \in [-N/2+1,\, N/2]$ for N even or $s \in [-(N-1)/2,\, (N-1)/2]$ for N odd, so that Eq. (A9) reads as

$$H_2 = \sum_{k\in \mathrm{FBZ}} \Bigg\{ \sum_{I\in\{A,B\}} \left[\Omega\, d_{Ik}^\dagger d_{Ik} + \frac{\Lambda}{2}(d_{Ik} d_{I,-k} + \mathrm{H.c.}) \right] + [J_k\,(d_{Ak}^\dagger d_{Bk} - d_{Ak}^\dagger d_{B,-k}^\dagger) + \mathrm{H.c.}] \Bigg\} \quad \text{(A11)}$$

with

$$J_k = \frac{\mu(\lambda-\omega)}{1+\mu}\left(\frac{1-\delta}{2} + \frac{1+\delta}{2}\, e^{-ik}\right). \quad \text{(A12)}$$

Introducing the normal mode operators $C_{\eta k}$ and $C_{\eta k}^\dagger$ defined, for $\eta \in \{+,-\}$, as

$$C_{\eta k} = \frac{1}{\sqrt{2}}\left(Z_{\eta Ak} + \eta\, \frac{J_k}{|J_k|}\, Z_{\eta Bk}\right), \quad \text{(A13)}$$

and the operators

$$Z_{\eta Ik} = \cosh\left(v_k^\eta\right) d_{Ik} + \sinh\left(v_k^\eta\right) d_{I,-k}^\dagger, \quad \text{(A14)}$$

with

$$\tanh\left(2v_k^\eta\right) = \frac{\Lambda - \eta\,|J_k|}{\Omega + \eta\,|J_k|}, \quad \text{(A15)}$$

the Hamiltonian (A11) is diagonalized as $H_2 = \sum_{k,\eta} \mathcal{E}_k^\eta\, C_{\eta k}^\dagger C_{\eta k}$, up to constant terms. The energy spectrum is therefore described by the two bands $\mathcal{E}_k^\pm$ defined by Eq. (9). Each $\mathcal{E}_k^\pm$ identifies a one-particle doubly degenerate excited level due to the $k \to -k$ symmetry. Notice the levels $k = 0, \pi$ have no degeneracy. The total number of levels is then reduced from $2N$ to $N+2$ for N even, or to $N+1$ for N odd.

From Eq. (9) one can easily show that the Gaussian Hamiltonian is positive definite, indeed $\mathcal{E}_k^\pm > 0$ for $\forall\, k \in \mathrm{FBZ}$ and $\mu < 1$. This indicates that the semiclassical solution (A8) is stable in the regime $\mu < 1$.

3. Topological invariant: Zak phase

For one-dimensional systems a widely employed topological invariant is the Zak phase defined by

$$\phi_{\mathrm{Zak}}^\eta = i\int_{-\pi}^{\pi} \frac{dk}{\pi}\, \langle G|C_{\eta k}\, \partial_k C_{\eta k}^\dagger|G\rangle. \quad \text{(A16)}$$

The definition of the operators $Z_{\eta Ik}$ given in (A14) has only real coefficients, therefore we can use (A13) and relate the Zak phase with the argument of $J_k = |J_k| e^{-i\theta_k}$, i.e.,

$$\phi_{\mathrm{Zak}}^\eta = \frac{\eta}{2\pi}\int_{-\pi}^{\pi} dk\, \partial_k\theta_k = \frac{\eta}{2\pi i}\oint_{J_k}\frac{dw}{w} = \eta\, \mathrm{Ind}_{J_k}(0), \quad \text{(A17)}$$

where $\mathrm{Ind}_{J_k}(0)$ is the winding number around the origin of the curve $J_k : (-\pi, \pi] \to \mathbb{C}$ and represents the total number of times that the curve travels counterclockwise around that point. Using Eq. (A12), we thus obtain

$$\delta > 0 \to \phi_{\mathrm{Zak}}^\eta = \eta \neq 0,$$
$$\delta < 0 \to \phi_{\mathrm{Zak}}^\eta = 0. \quad \text{(A18)}$$

This implies that in the SSB regime $\lambda \gg \omega$ for $\mu < 1$, the chain enters a topological nontrivial phase when $\delta > 0$ ($\epsilon_2 > \epsilon_1$). At the topological phase transition the band gap vanishes according to Eq. (9).

APPENDIX B: OPEN CHAIN

Here we provide calculations for the chain with OBC and investigate the emergence of edge states.

1. Quadratic Hamiltonian

For OBC, it is useful to rewrite the quadratic Hamiltonian (8) as

$$H_2 = \sum_{In,I'n'} \Big[X_{In,I'n'}\, d_{In}^\dagger d_{I'n'} + \frac{1}{2}(Y_{In,I'n'}\, d_{In}^\dagger d_{I'n'}^\dagger + Y_{In,I'n'}^*\, d_{In} d_{I'n'}) \Big], \quad \text{(B1)}$$

with the matrix elements $X_{In,I'n'}$ and $Y_{In,I'n'}$ related to the semiclassical ground state given in Eq. (A6). In this way H_2 can be diagonalized via a Bogoliubov transformation introducing the $4N \times 4N$ matrix

$$\mathcal{L} = \begin{pmatrix} X & Y \\ -Y^* & -X^* \end{pmatrix} \quad \text{(B2)}$$

and numerically calculating its spectrum $\mathcal{L}\,\vec{u}_\nu = \mathcal{E}_\nu \vec{u}_\nu$, with $\vec{u}_\nu = (u_{Inv}, \widetilde{u}_{Inv})$, $\sum_{In}(\,|u_{Inv}|^2 - |\widetilde{u}_{Inv}|^2\,) = 1$.

The positive eigenvalues $\mathcal{E}_\nu$ identify the energy levels of H_2, that can be therefore expressed as $H_2 = \sum_\nu \mathcal{E}_\nu C_\nu^\dagger C_\nu + \mathcal{E}_0$, with $C_\nu = \sum_{In}(u_{Inv} d_{In} - \widetilde{u}_{Inv} d_{In}^\dagger)$ and $\mathcal{E}_0$ a constant term. The emerging energy spectrum is plotted in Fig. 3(c) and the

eigenstates $\vec{u}_\nu$ solve the following equations:

$$\begin{aligned}
&\Omega_{An}\, u_{An} + \Lambda_{An}\, \widetilde{u}_{An} + J_{1n}(u_{Bn} - \widetilde{u}_{Bn}) + J_{2n}(u_{Bn-1} - \widetilde{u}_{Bn-1}) = \mathcal{E}\, u_{An},\\
&\Omega_{Bn}\, u_{Bn} + \Lambda_{Bn}\, \widetilde{u}_{Bn} + J_{1n}(u_{An} - \widetilde{u}_{An}) + J_{2n}(u_{An+1} - \widetilde{u}_{An+1}) = \mathcal{E}\, u_{Bn},\\
&\Omega_{An}\, \widetilde{u}_{An} + \Lambda_{An}\, u_{An} - J_{1n}(u_{Bn} - \widetilde{u}_{Bn}) - J_{2n}(u_{Bn-1} - \widetilde{u}_{Bn-1}) = -\mathcal{E}\, \widetilde{u}_{An},\\
&\Omega_{Bn}\, \widetilde{u}_{Bn} + \Lambda_{Bn}\, u_{Bn} - J_{1n}(u_{An} - \widetilde{u}_{An}) - J_{2n}(u_{An+1} - \widetilde{u}_{An+1}) = -\mathcal{E}\, \widetilde{u}_{Bn},
\end{aligned} \tag{B3}$$

where we removed the index ν for the sake of a lighter notation and we used the site-dependent parameters Ω_{In}, Λ_{In}, and J_{In} defined below Eq. (8). In the case of PBC the parameters reduce to Eqs. (A10). In the bulk region Eq. (B3) can be unraveled to obtain

$$u_{An+1} + u_{An-1} + 2\cosh\left(\frac{1}{\xi}\right) u_{An} = 0, \tag{B4}$$

$$\widetilde{u}_{An} = \frac{\mathcal{E} - \lambda}{\mathcal{E} + \lambda}\, u_{An}$$

with

$$\cosh^2\left(\frac{1}{2\xi}\right) = \frac{1 - \chi^2}{1 - \delta^2}, \quad \chi = \frac{1}{\mu} - \left(\frac{1}{\mu} + 1\right)\frac{\mathcal{E}^2}{\omega_H^2}. \tag{B5}$$

Analogous equations hold for u_{Bn}, $\widetilde{u}_{Bn}$. Equation (B4) is solved by

$$u_{An} = (-1)^n \left(w_1\, e^{-n/\xi} + w_2\, e^{n/\xi}\right), \tag{B6}$$

where the constants w_1 and w_2 can be fixed imposing Eq. (B3) right outside the bulk region. The solution (B6) describes either localized or extended modes depending on whether ξ being real or imaginary. According to Eq. (B5), it can be shown that

$$\xi \in \mathbb{R} \iff \mathcal{E}^-_{k=\pi} < \mathcal{E} < \mathcal{E}^+_{k=\pi}, \tag{B7}$$

namely, an eigenstate is localized if and only if the related energy lies inside the band gap. In this case the localization length is given by Eq. (B5). As shown by Fig. 3(c), the OBC energy spectrum does not feature isolated levels inside the band gap. Therefore, even when $\delta > 0$, the system does not possess localized edge modes.

2. Death and revival of edge states via an effective model

The disappearance of edges states in the topological phase can be understood by considering the spectrum at $\delta = 1$. In this case, the chain is composed of $N - 1$ resonator pairs, forming the bulk, and of two isolated sites at the edges. Each bulk pair contains two modes, the Higgs-like mode with energy ω_H and the Goldstone-like mode with energy $\omega_H \sqrt{(1-\mu)/(1+\mu)}$. The edge sites have instead a single mode with energy ω_H so that, at $\delta = 1$, the edge modes and the Higgs-like bulk modes are degenerate. In this scenario any finite value of ϵ_1 ($\delta \lesssim 1$) couples all degenerate modes causing the spreading of the edge modes across the whole chain. To illustrate this point we consider the following model:

$$H_2^{\text{eff}} = \omega_H \sum_{l=1}^{N+1} \zeta_l^\dagger \zeta_l + t \sum_{l=1}^{N} (\zeta_l^\dagger\, \zeta_{l+1} + \zeta_l\, \zeta_{l+1}^\dagger) \tag{B8}$$

with

$$\begin{cases} \zeta_1, \zeta_{N+1} \to \text{edge creation operators}, \\ \zeta_{l=2,\ldots,N} \to \text{bulk creation operators}. \end{cases}$$

Writing Eq. (B8) in the form (B1), the matrix Y vanishes and X is a Toepliz tridiagonal matrix which can be exactly diagonalized so that $H_2^{\text{eff}} = \sum_\nu E_\nu \gamma_\nu^\dagger \gamma_\nu$, with

$$E_\nu = \omega_H + 2t\cos\left(\frac{\pi\nu}{N+2}\right), \tag{B9}$$

$$\gamma_\nu = \sqrt{\frac{2}{N+2}} \sum_{l=1}^{N+1} \sin\left(\frac{\pi\nu}{N+2}\right)\zeta_l, \tag{B10}$$

for $\nu = 1, \ldots, N+1$. All γ_ν modes are thus delocalized across the chain. This behavior is ultimately rooted in the degeneracy of all the modes for $t = 0$.

A drastic change happens when introducing a small correction δ_{ω_H} to the edge energies via

$$\delta H_2^{\text{eff}} = -\delta_{\omega_H}(\zeta_1^\dagger\, \zeta_1 + \zeta_{N+1}^\dagger\, \zeta_{N+1}). \tag{B11}$$

In this case, using second-order perturbation theory for $t \ll \delta_{\omega_H}$, the energy of the edge modes becomes

$$E_e = \omega_H - \delta_{\omega_H} - \frac{t^2}{\delta_{\omega_H}} + o(t^3). \tag{B12}$$

Solving the eigenvalues equation for $H_2^{\text{eff}} + \delta H_2^{\text{eff}}$, it is easy to show that, being $E_e < \omega_H$, the corresponding mode is exponentially localized.

3. Lowering the driving at the boundaries

The energy ω_H of the edge modes at $\delta = 1$ depends on the driving intensity λ. It can be thus reduced by appropriately decreasing the driving at the chain boundaries by an amount δ_λ. This reduction is achieved by introducing a correction δH_λ to the Hamiltonian as in Eq. (11). In this way, for $\lambda \gg \omega$, we obtain a nonvanishing δ_{ω_H} leading to the emergence of two isolated modes in the spectrum of the quadratic Hamiltonian, as shown in Fig. 4(a). These two modes appear both in the topological and in the trivial phase, around $\delta = 1$ and -1, and lie in the band gap. They are thus localized according to Eq. (B5). However, in the two phases, the localization arises from different mechanisms.

(i) *Topological phase.* When $\delta = 1$ ($\epsilon_1 = 0$), the semiclassical ground state is inhomogeneous for $\delta_\lambda = 0$. In particular the length (A1) tends to zero and the inhomogeneity is confined to the first and last sites, i.e., $|\alpha_1| = |\beta_N| = g > \bar{g} = |\alpha_{n\neq 1}| = |\beta_{n\neq N}|$ as in Fig. 7. According to Eq. (8) of the main text, the energy of edge and bulk modes can be obtained

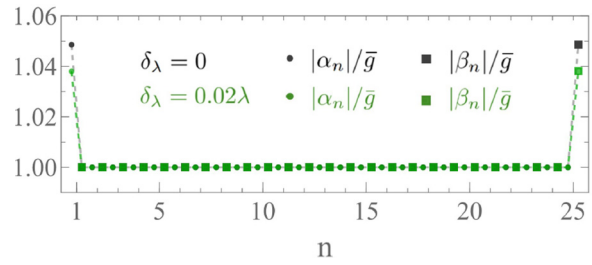

FIG. 7. The OBC semiclassical ground states for $N = 25$, $\delta = 1$, and $\delta_\lambda = 0$ (black) or $\delta_\lambda = 0.02\,\lambda$ (green).

diagonalizing the following Hamiltonians:

$$H_{\text{edge}}^{(\delta=1)} = \Omega_e\, d^\dagger d + \frac{\Lambda_e}{2}\,(dd + d^\dagger d^\dagger) \tag{B13}$$

with

$$\begin{cases} \Omega_e = \lambda + 2\epsilon_L \bar{g}^2, \\ \Lambda_e = \lambda - 2\epsilon_L \bar{g}^2, \end{cases}$$

for the edge sites $d \in \{d_{A1}, d_{BN}\}$, and

$$H_{\text{bulk}}^{(\delta=1)} = \Omega\,(d_A^\dagger d_A + d_B^\dagger d_B) + \frac{\Lambda}{2}\,(d_A d_A + d_B d_B + \text{H.c.}) + J_2\,(d_A^\dagger d_B - d_A d_B + \text{H.c.}) \tag{B14}$$

with

$$\begin{cases} \Omega = \lambda + 2\epsilon_L \bar{g}^2\,, \\ \Lambda = \lambda - 2\epsilon_L \bar{g}^2\,, \\ J_2 = \epsilon_2\,\bar{g}^2\,, \end{cases}$$

for the bulk pairs $(d_B, d_A) \in \{(d_{Bn}, d_{An+1})\}_{n=1,\ldots,N-1}$. Introducing normal modes through Bogoliubov transformations, each bulk pair contains a mode with energy ω_H identical to that of the edge modes. The specific inhomogeneous structure of the semiclassical solution in the bulk and in the edges, quantified by the ratio $g/\bar{g}$, leads to degenerate bulk and edges modes in the Gaussian Hamiltonian. When the driving at the boundaries is decreased, the inhomogeneity is reduced (see Fig. 7) via

$$|\alpha_1| = |\beta_N| = g\sqrt{1 - \frac{\delta_\lambda}{\lambda - \omega}}, \tag{B15}$$

and, as in Fig. 4(a), the energy of the edge modes becomes

$$\omega_e^{(\delta=1)} = \omega_H \sqrt{\left(1 - \frac{\delta_\lambda}{\lambda}\right)\left(1 - \frac{\delta_\lambda}{\lambda - \omega}\right)} < \omega_H. \tag{B16}$$

In this scenario, introducing a small finite value of ϵ_1 does not couple edge and bulk modes. The former are thus topologically protected modes, localized according to Eq. (B5). As long as δ_λ is not too small, the localization length stays well defined in the entire topological phase $\delta > 0$, and exhibits an "SSH behavior" $\xi^{-1} \sim \log(\frac{1+\delta}{1-\delta})$ [see Figs. 4(b) and 8]. More precisely, following Eq. (B5), this behavior emerges when $\chi \sim 0 \Leftrightarrow \mathcal{E} \sim (1+\mu)^{-1/2}$, meaning that the edge state energy lies in the center of the band gap. Notice that, in the SSH model, δ represents the imbalance between intercell and intracell quadratic tunnelings, whereas, in our case, it corresponds to the imbalance of nonlinear cross-Kerr interactions.

Let us highlight that δ_λ cannot be nevertheless too large, as this would cause the edge energy at $\delta = 1$ to fall outside the band gap, crossing the upper edge of the lower band. Notice that so far we considered the case $\mu \ll 1$. As μ increases, the bulk region shrinks (see Fig. 5) and restoring the edge states requires a reduction of the driving intensities on all sites affected by the inhomogeneity.

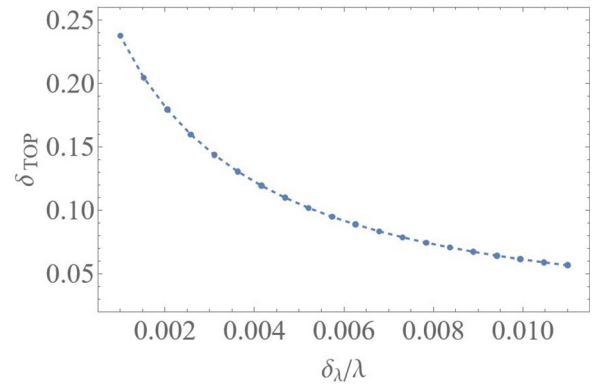

FIG. 8. The value δ_{TOP} below which the localization length of the two modes appearing in the band gap exceeds half the chain length $N/2$ ($\mu = 0.1$ and $N = 25$). Considering Eq. (B6), if $\delta > \delta_{\text{TOP}}$, the modes can be considered localized.

(ii) *Trivial phase.* When $\delta = -1$ ($\epsilon_2 = 0$), the semiclassical ground state, for $\delta_\lambda = 0$, is homogeneous, i.e., $|\alpha_n| = |\beta_n| = \bar{g}$ as in Fig. 9. The entire chain, consisting of N decoupled pairs, can thus be considered bulk. According to Eq. (8), the energy of all the pairs can be obtained diagonalizing the following Hamiltonian:

$$H_{\text{bulk}}^{(\delta=-1)} = \Omega\,(d_A^\dagger d_A + d_B^\dagger d_B) + \frac{\Lambda}{2}\,(d_A d_A + d_B d_B + \text{H.c.}) + J_1\,(d_A^\dagger d_B - d_A d_B + \text{H.c.}) \tag{B17}$$

with

$$\begin{cases} \Omega = \lambda + 2\epsilon_L \bar{g}^2, \\ \Lambda = \lambda - 2\epsilon_L \bar{g}^2, \\ J_1 = \epsilon_1\,\bar{g}^2, \end{cases}$$

and $(d_B, d_A) \in \{(d_{Bn}, d_{An})\}_{n=1,\ldots,N}$. The normal modes of all the pairs are thus degenerate and any small finite value of ϵ_2 couples nearest-neighbor pairs spreading all the modes across the whole chain according to Eq. (B9). In this case, decreasing the driving at the boundaries introduces an impurity in the first and last pairs, making the semiclassical ground states inhomogeneous (see Fig. 9). The semiclassical solution on the

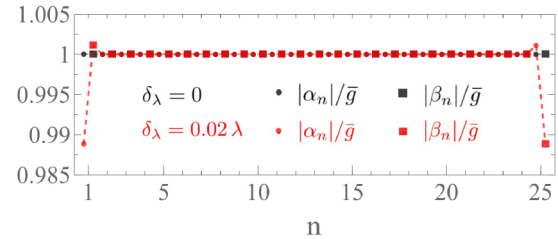

FIG. 9. The OBC semiclassical ground states for $N = 25$, $\delta = -1$, and $\delta_\lambda = 0$ (black) or $\delta_\lambda = 0.02\,\lambda$ (red).

boundary sites can be cast as

$$|\alpha_1| = |\beta_N| = \bar{g}\sqrt{1 - \tfrac{\delta_\lambda}{(1-\mu)(\lambda-\omega)}}, \qquad |\beta_2| = |\alpha_{N-1}| = \bar{g}\sqrt{1 + \tfrac{\mu\,\delta_\lambda}{(1-\mu)(\lambda-\omega)}} \tag{B18}$$

yielding two spurious boundary modes with energy

$$\omega_{\text{spur}}^{(\delta=-1)} = \omega_H\left(1 - \frac{2\lambda-\omega}{4(\lambda-\omega)}\,\frac{\delta_\lambda}{\lambda} + o\left(\frac{\delta_\lambda}{\lambda}\right)^2\right) < \omega_H, \tag{B19}$$

which, as in Fig. 4(a), lie in band gap. Therefore, also in this scenario, introducing a small finite interaction ϵ_2 between the pairs does not couple boundary and bulk modes. The former are thus localized according to Eq. (B5). Anyway the localization is here induced by the impurity, and it is not related to topology. This different nature is captured by the behavior of the localization length [see Fig. 4(b)], which can be estimated via Eqs. (B5) and (B12):

$$\xi_{\text{spur}}^{-1} \sim 2\,\text{arcosh}\sqrt{\frac{1 - \frac{1}{\mu^2}\left[1 - (1+\mu)\left(1 - \frac{\delta_\lambda}{2\lambda} - \frac{\lambda}{8\,\delta_\lambda}\left(\frac{\mu\,(1+\delta)}{1+\mu}\right)^2\right)^2\right]^2}{1-\delta^2}}, \tag{B20}$$

where we assumed $\omega = 0$ ($\lambda \gg \omega$) for the sake of a lighter notation.

In Fig. 4(b), the dots are obtained via numerical exponential fits of the Hamiltonian eigenstates and the dashed lines combining Eq. (B5) with numerical eigenvalues. The solid lines are analytical estimations given by the "SSH behavior" in the topological phase, or by perturbation theory in the trivial phase, as in Eq. (B20).

The length (B20) becomes imaginary when the energy of the spurious modes crosses the lower edge of the upper band. This happens if $J_2 \gtrsim \delta_\lambda$ when the interaction becomes high enough to overcome the impurity. Therefore, when $\delta > \delta_{\text{spur}}$ with

$$\delta_{\text{spur}} \sim -1 + 2\left(\frac{1}{\mu} + 1\right)\frac{\delta_\lambda}{\lambda}, \tag{B21}$$

as shown in Fig. 10, spurious modes lose their localization and spread across the chain. Unlike the edge modes appearing in the topological phase, these boundary modes are thus not localized throughout the entire trivial phase, but instead exhibit a threshold δ_{spur} beyond which localization is lost.

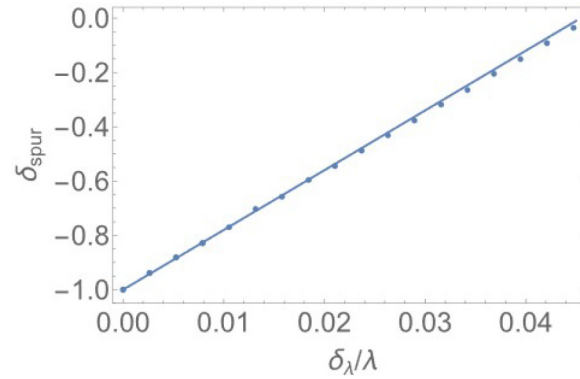

FIG. 10. The threshold value δ_{spur} above which the energy of the boundary spurious modes violates Eq. (B7) causing their spreading across the chain. The solid line is the analytical estimation given by Eq. (B21).

[1] S. Sachdev, *Quantum Phase Transitions* (Cambridge University Press, Cambridge, 2011).

[2] A. Kitaev, V. Lebedev, and M. Feigel'man, Periodic table for topological insulators and superconductors, AIP Conf. Proc. **1134**, 22 (2009).

[3] M. Z. Hasan and C. L. Kane, Colloquium: Topological insulators, Rev. Mod. Phys. **82**, 3045 (2010).

[4] C. K. Chiu, J. C. Y. Teo, A. P. Schnyder, and S. Ryu, Classification of topological quantum matter with symmetries, Rev. Mod. Phys. **88**, 035005 (2016).

[5] C. Kane, Topological band theory and the $\mathbb{Z}_2$ invariant, in *Topological Insulators* (Elsevier, Amsterdam, 2013), Chap. 1, pp. 3–34.

[6] T. Ozawa, H. M. Price, A. Amo, N. Goldman, M. Hafezi, L. Lu, M. C. Rechtsman, D. Schuster, J. Simon, O. Zilberberg, and I. Carusotto, Topological photonics, Rev. Mod. Phys. **91**, 015006 (2019).

[7] D. J. Thouless, M. Kohmoto, M. P. Nightingale, and M. den Nijs, Quantized Hall conductance in a two-dimensional periodic potential, Phys. Rev. Lett. **49**, 405 (1982).

[8] D. J. Thouless, Quantization of particle transport, Phys. Rev. B **27**, 6083 (1983).

[9] R. Jackiw and C. Rebbi, Solitons with fermion number, Phys. Rev. D **13**, 3398 (1976).

[10] Y. Hatsugai, Chern number and edge states in the integer quantum Hall effect, Phys. Rev. Lett. **71**, 3697 (1993).

[11] S. Rachel, Interacting topological insulators: A review, Rep. Prog. Phys. **81**, 116501 (2018).

[12] M. Jürgensen, S. Mukherjee, C. Jörg, and M. C. Rechtsman, Quantized fractional Thouless pumping of solitons, Nat. Phys. **19**, 420 (2023).

[13] N. Mostaan, F. Grusdt, and N. Goldman, Quantized topological pumping of solitons in nonlinear photonics and ultracold atomic mixtures, Nat. Commun. **13**, 5997 (2022).

[14] K. Sone, E. Motohiko, A. Yuto, Y. Nobuyuki, and S. Takahiro, Nonlinearity-induced topological phase transition characterized by the nonlinear Chern number, Nat. Phys. **20**, 1164 (2024).

[15] L. Jezequel and P. Delplace, Nonlinear edge modes from topological one-dimensional lattices, Phys. Rev. B **105**, 035410 (2022).

[16] T. Isobe, T. Yoshida, and Y. Hatsugai, Bulk-Edge correspondence for nonlinear eigenvalue problems, Phys. Rev. Lett. **132**, 126601 (2024).

[17] M. Brunelli, C. C. Wanjura, and A. Nunnenkamp, Restoration of the non-Hermitian bulk-boundary correspondence via topological amplification, SciPost Phys. **15**, 173 (2023).

[18] X. G. Wen and Q. Niu, Ground-state degeneracy of the fractional quantum Hall states in the presence of a random potential and on high-genus Riemann surfaces, Phys. Rev. B **41**, 9377 (1990).

[19] A. Kitaev and J. Preskill, Topological entanglement entropy, Phys. Rev. Lett. **96**, 110404 (2006).

[20] M. Levin and X. G. Wen, Detecting topological order in a ground state wave function, Phys. Rev. Lett. **96**, 110405 (2006).

[21] W. P. Su and J. R. Schrieffer, Fractionally charged excitations in charge-density-wave systems with commensurability 3, Phys. Rev. Lett. **46**, 738 (1981).

[22] D. Arovas, J. R. Schrieffer, and F. Wilczek, Fractional statistics and the quantum Hall effect, Phys. Rev. Lett. **53**, 722 (1984).

[23] X. G. Wen, Topological orders and edge excitations in fractional quantum Hall states, in *Field Theory, Topology and Condensed Matter Physics* (Springer, Berlin, 1995), pp. 155–176.

[24] L. Lu, J. Joannopoulos, and M. Soljačić, Topological photonics, Nat. Photon. **8**, 821 (2014).

[25] I. Carusotto and C. Ciuti, Quantum fluids of light, Rev. Mod. Phys. **85**, 299 (2013).

[26] X. Gu, A. F. Kockum, A. Miranowicz, Y. Liu, and F. Nori, Microwave photonics with superconducting quantum circuits, Phys. Rep. **718-719**, 1 (2017).

[27] M. Fitzpatrick, N. M. Sundaresan, A. C. Y. Li, J. Koch, and A. A. Houck, Observation of a Dissipative phase transition in a one-dimensional circuit QED lattice, Phys. Rev. X **7**, 011016 (2017).

[28] P. Brookes, G. Tancredi, A. D. Patterson, J. Rahamim, M. Esposito, T. K. Mavrogordatos, P. J. Leek, E. Ginossar, and M. H. Szymanska, Critical slowing down in circuit quantum electrodynamics, Sci. Adv. **7**, eabe9492 (2021).

[29] Q. Chen, M. Fischer, Y. Nojiri, M. Renger, E. Xie, M. Partanen, S. Pogorzalek, K. G. Fedorov, A. Marx, F. Deppe, and R. Gross, Quantum behavior of a superconducting Duffing oscillator at the dissipative phase transition, Nat. Commun. **14**, 2896 (2023).

[30] R. H. Zheng, W. Ning, Y. H. Chen, J. H. Lü, L. T. Shen, K. Xu, Y. R. Zhang, D. Xu, H. Li, Y. Xia, F. Wu, Z. B. Yang, A. Miranowicz, N. Lambert, D. Zheng, H. Fan, F. Nori, and S. B. Zheng, Observation of a superradiant phase transition with emergent cat states, Phys. Rev. Lett. **131**, 113601 (2023).

[31] G. Beaulieu, F. Minganti, S. Frasca, V. Savona, S. Felicetti, R. Di Candia, and P. Scarlino, Observation of first- and second-order dissipative phase transitions in a two-photon driven Kerr resonator, Nat. Commun. **16**, 1954 (2025).

[32] H. J. Carmichael, Breakdown of photon blockade: A dissipative quantum phase transition in zero dimensions, Phys. Rev. X **5**, 031028 (2015).

[33] W. Casteels, F. Storme, A. Le Boité, and C. Ciuti, Power laws in the dynamic hysteresis of quantum nonlinear photonic resonators, Phys. Rev. A **93**, 033824 (2016).

[34] N. Bartolo, F. Minganti, W. Casteels, and C. Ciuti, Exact steady state of a kerr resonator with one- and two-photon driving and dissipation: Controllable Wigner-function multimodality and dissipative phase transitions, Phys. Rev. A **94**, 033841 (2016).

[35] M. I. Dykman, *Fluctuating Nonlinear Oscillators: From Nanomechanics to Quantum Superconducting Circuits* (Oxford University Press, Oxford, 2012).

[36] F. Minganti, L. Garbe, A. Le Boité, and S. Felicetti, Non-Gaussian superradiant transition via three-body ultrastrong coupling, Phys. Rev. A **107**, 013715 (2023).

[37] S. Ashhab, Superradiance transition in a system with a single qubit and a single oscillator, Phys. Rev. A **87**, 013826 (2013).

[38] M. J. Hwang, R. Puebla, and M. B. Plenio, Quantum phase transition and universal dynamics in the Rabi model, Phys. Rev. Lett. **115**, 180404 (2015).

[39] J. Peng, E. Rico, J. Zhong, E. Solano, and I. L. Egusquiza, Unified superradiant phase transitions, Phys. Rev. A **100**, 063820 (2019).

[40] S. Felicetti and A. Le Boité, Universal spectral features of ultrastrongly coupled systems, Phys. Rev. Lett. **124**, 040404 (2020).

[41] M. Poot and H. S. van der Zant, Mechanical systems in the quantum regime, Phys. Rep. **511**, 273 (2012).

[42] P. D. Drummond and D. F. Walls, Quantum theory of optical bistability. I. Nonlinear polarisability model, J. Phys. A: Math. Gen. **13**, 725 (1980).

[43] C. Arenz, C. Cormick, D. Vitali, and G. Morigi, Generation of two-mode entangled states by quantum reservoir engineering, J. Phys. B: At. Mol. Opt. Phys. **46**, 224001 (2013).

[44] P. Drummond, K. McNeil, and D. Walls, Non-equilibrium transitions in sub/second harmonic generation, Int. J. Opt. **28**, 211 (1981).

[45] M. Calvanese Strinati and C. Conti, Non-Gaussianity in the quantum parametric oscillator, Phys. Rev. A **109**, 063519 (2024).

[46] S. Puri, S. Boutin, and A. Blais, Engineering the quantum states of light in a Kerr-nonlinear resonator by two-photon driving, npj Quantum Inf. **3**, 18 (2017).

[47] H. Goto, Quantum computation based on quantum adiabatic bifurcations of Kerr-nonlinear parametric oscillators, J. Phys. Soc. Jpn. **88**, 061015 (2019).

[48] A. Grimm, N. E. Frattini, S. Puri, S. O. Mundhada, S. Touzard, M. Mirrahimi, S. M. Girvin, S. Shankar, and M. H. Devoret, Stabilization and operation of a Kerr-cat qubit, Nature (London) **584**, 205 (2020).

[49] R. Di Candia, F. Minganti, K. V. Petrovnin, G. S. Paraoanu, and S. Felicetti, Critical parametric quantum sensing, npj Quantum Inf. **9**, 23 (2023).

[50] G. Beaulieu, F. Minganti, S. Frasca, M. Scigliuzzo, S. Felicetti, R. Di Candia, and P. Scarlino, Criticality-enhanced quantum sensing with a parametric superconducting resonator, PRX Quantum **6**, 020301 (2025).

[51] K. Petrovnin, J. Wang, M. Perelshtein, P. Hakonen, and G. S. Paraoanu, Microwave photon detection at parametric criticality, PRX Quantum **5**, 020342 (2024).

[52] A. Gu, J. Sloan, C. Roques-Carmes, S. Choi, E. I. Rosenthal, M. Horodynski, Y. Salamin, J. Vučković, and M. Soljačić, Quantum sensitivity of parametric oscillators, Phys. Rev. Res. **7**, L022056 (2025).

[53] T. Kanao and H. Goto, High-accuracy Ising machine using Kerr-nonlinear parametric oscillators with local four-body interactions, npj Quantum Inf. **7**, 18 (2021).

[54] P. Zapletal, A. Nunnenkamp, and M. Brunelli, Stabilization of multimode Schrödinger cat states via normal-mode dissipation engineering, PRX Quantum **3**, 010301 (2022).
[55] M. Calvanese Strinati and C. Conti, Multidimensional hyperspin machine, Nat. Commun. **13**, 7248 (2022).
[56] U. Alushi, A. Coppo, V. Brosco, R. Di Candia, and S. Felicetti, Collective quantum enhancement in critical quantum sensing, Commun. Phys. **8**, 74 (2025).
[57] F. Caleffi, M. Capone, and I. Carusotto, Collective excitations of a strongly correlated nonequilibrium photon fluid across the insulator-superfluid phase transition, Phys. Rev. Lett. **131**, 193604 (2023).
[58] A. Roy, M. Parto, R. Nehra, C. Leefmans, and A. Marandi, Topological optical parametric oscillation, Nanophotonics **11**, 1611 (2022).
[59] L. X. Guo, L. L. Wan, L. G. Si, and Y. Wu, Topological amplification and frequency conversion in a photonic lattice with a two-photon driving, Phys. Rev. A **108**, 013512 (2023).
[60] T. Goren, K. Plekhanov, F. Appas, and K. Le Hur, Topological Zak phase in strongly coupled LC circuits, Phys. Rev. B **97**, 041106(R) (2018).
[61] D. Leykam and Y. D. Chong, Edge solitons in nonlinear-photonic topological insulators, Phys. Rev. Lett. **117**, 143901 (2016).
[62] Y. Hadad, A. B. Khanikaev, and A. Alù, Self-induced topological transitions and edge states supported by nonlinear staggered potentials, Phys. Rev. B **93**, 155112 (2016).
[63] K. Sone and Y. Hatsugai, Topological-to-topological transition induced by on-site nonlinearity in a one-dimensional topological insulator, Phys. Rev. Res. **8**, L012045 (2026).
[64] S. Ravets, N. Pernet, N. Mostaan, N. Goldman, and J. Bloch, Thouless pumping in a driven-dissipative Kerr resonator array, Phys. Rev. Lett. **134**, 093801 (2025).
[65] C. E. Bardyn, T. Karzig, G. Refael, and T. C. H. Liew, Chiral Bogoliubov excitations in nonlinear bosonic systems, Phys. Rev. B **93**, 020502(R) (2016).
[66] L. Rassaert, T. Ramos, T. Roscilde, and D. Porras, Emerging non-Hermitian topology in a chiral-driven-dissipative Bose-Hubbard model, Phys. Rev. Lett. **135**, 203603 (2025).
[67] W. P. Su, J. R. Schrieffer, and A. J. Heeger, Solitons in polyacetylene, Phys. Rev. Lett. **42**, 1698 (1979).
[68] F. Hellbach, D. De Bernardis, M. Saur, I. Carusotto, W. Belzig, and G. Rastelli, Nonlinearity-induced symmetry breaking in a system of two parametrically driven Kerr-Duffing oscillators, New J. Phys. **26**, 103020 (2024).
[69] T. D. Kühner and H. Monien, Phases of the one-dimensional Bose-Hubbard model, Phys. Rev. B **58**, R14741 (1998).
[70] D. Rossini and R. Fazio, Phase diagram of the extended Bose-Hubbard model, New J. Phys. **14**, 065012 (2012).
[71] Y. Hwang, J. Ahn, and B.-J. Yang, Fragile topology protected by inversion symmetry: Diagnosis, bulk-boundary correspondence, and wilson loop, Phys. Rev. B **100**, 205126 (2019).
[72] P. Delplace, Berry-Chern monopoles and spectral flows, SciPost Phys. Lect. Notes, 39 (2022).
[73] M. Peskin and D. Schroeder, *An Introduction To Quantum Field Theory* (CRC Press, Boca Raton, FL, 1995).
[74] M. Schwartz, *Quantum Field Theory and the Standard Model* (Cambridge University Press, Cambridge, 2014).
[75] A. Amaricci, L. Privitera, F. Petocchi, M. Capone, G. Sangiovanni, and B. Trauzettel, Edge state reconstruction from strong correlations in quantum spin Hall insulators, Phys. Rev. B **95**, 205120 (2017).
[76] A. Valli, A. Amaricci, V. Brosco, and M. Capone, Quantum interference assisted spin filtering in graphene nanoflakes, Nano Lett. **18**, 2158 (2018).
[77] M.-J. Hwang, P. Rabl, and M. B. Plenio, Dissipative phase transition in the open quantum rabi model, Phys. Rev. A **97**, 013825 (2018).
[78] M. Cai, Z. Liu, W.-D. Zhao, Y. Wu, Q. Mei, Y. Jiang, L. He, X. Zhang, Z. Zhou, and L. Duan, Observation of a quantum phase transition in the quantum Rabi model with a single trapped ion, Nat. Commun. **12**, 1126 (2021).